

STUDY OF FINE-SCALE VORTICAL STRUCTURES IN A VON KÁRMÁN MIXING FLOW

Farid Aligolzadeh

Department of Energy and Process Engineering
Norwegian University of Science and Technology
NO-7491, Trondheim, Norway
farid.aligolzadeh@ntnu.no

Markus Holzner

Swiss Federal Institute of Forest,
Snow and Landscape Research WSL
8903 Birmensdorf, Switzerland
Swiss Federal Institute of Aquatic Science
and Technology Eawag
8600 Dübendorf, Switzerland
holzner@ifu.baug.ethz.ch

James R. Dawson

Department of Energy and Process Engineering
Norwegian University of Science and Technology
NO-7491, Trondheim, Norway
james.r.dawson@ntnu.no

ABSTRACT

Intense small-scale vortical structures also known as ‘filaments’ or ‘worms’ have been studied in a wide range of turbulent flows, mostly using DNS. In the present study, we investigate vorticity dynamics of vortex filaments at the dissipation scale in a fully resolved three-dimensional experimental data set of a turbulent mixing flow measured at the center of a large von Kármán mixing tank at a $Re_\lambda = 179$. To avoid arbitrariness inherent to threshold-dependent detection criteria and dependence of the results on the observer, an objective vortex detection method proposed by Haller *et al.* (2016) is implemented. One thousand instantaneous 3D velocity fields are studied. These fields were measured at random times with a spatial resolution of 1η , where η is the Kolmogorov length scale. About 12500 structures were detected having an average radius of 5.1η , which is similar to previous findings on vortex filaments in HIT and turbulent jets and channels. Local features related to the structures and global features of the flow were investigated and compared. Structures are characterized by high vorticity and low strain and the vorticity vector is predominantly aligned with the intermediate strain eigenvector that has a positive eigenvalue on average. The vorticity vector is predominantly oriented normally to the compressive and extensional strain eigenvectors suggesting that the structures are quasi one-dimensional and shows that enstrophy production inside the structures results from vortex stretching. We further investigate the mechanisms that sustain the vortical structures by treating them as turbulent structures embedded in a less turbulent ambient flow, analogous to a turbulent flow separated by a turbulent/nonturbulent interface from its quiescent surroundings, and we analyze the entrainment/detrainment across their boundaries. This analysis shows that the structures are entraining ambient fluid on average in radial direction and that this entrainment is a result of the competing effects of non-viscous and viscous phenomena consistent with Burgers’ vortex model.

Introduction/Motivation

In turbulent flows, vortical structures are defined as regions of concentrated enstrophy with a life time larger than the characteristic time scale of the flow (Dubief & Delcayre, 2000). Intense vortical structures (IVSs) at the dissipation scale, often called *worms* or *filaments*, have shown universal features among a variety of different turbulent flows such as homogeneous isotropic turbulence (Jiménez *et al.*, 1993; Jiménez & Wray, 1998), jets (Ganapathisubramani *et al.*, 2008; da Silva *et al.*, 2011), channel flows (Kang *et al.*, 2009), stratified flows (Neamtu-Halic *et al.*, 2021). These studies have shown that worms or vortex filaments have a radius of about 5η , where $\eta = (\frac{\nu^3}{\epsilon})^{1/4}$ is the Kolmogorov length scale. In the DNS study of Jiménez *et al.* (1993) it was shown that stretching, $\alpha = \omega_i \omega_j s_{ij} / \omega^2$, is relatively low in small-scale vortices which indicates lack of self-amplification. The lack of self-amplification means that the vortices are passive and decoupled from the straining field of the flow. The worms are sustained by the strain field of the flow but the strain field is not affected by the presence of the worms. So, the worms are the consequence of turbulence dynamics and not important in evolution of the dynamics. For larger size vortices the strain field and the vortices show a two-way interaction with each other. The strain field is modified by the presence of the large scale vortices and the modified strain field modifies back the vortices. So on the contrary to small scale vortices, the large scale vortices are dynamically important in evolution of turbulence (Tsinober, 2009). Despite the many efforts to understand the importance and interactions of vortical structures with the surrounding flow, our understanding is still incomplete. In particular, the way vortical structures exchange mass, momentum and vorticity with the surrounding fluid has remained obscure. We show that fine-scale vortical structures are by no means passive in the sense of exchange, i.e. they interact with the background flow by entraining (detraining) mass radially (axially) and are thus not frozen to the flow or passively advected.

In addition to the inherent difficulty in obtaining fully resolved volumetric time-resolved measurements, there is the additional challenge of robust identification of high enstrophy structures. The intense vortical structures are usually detected by using a threshold on the norm of the vorticity field or the intensity of vorticity relative to the strain field, which are not objective detection methods. That is, besides the dependence on a user-dependent threshold, the results also depend on the observer, i.e. a change of reference system will yield different structures. In this study, we use a recent method proposed by Haller *et al.* (2016) based on the *vorticity deviation* to objectively detect the structures in our experimental data set. The method isolates a coherent fluid volume, in which fluid elements complete equal bulk material rotation relative to the mean rotation. The resulting coherent structures do not change with reference system and are truly objective. Recently, the method has been successfully applied to 3D turbulence (Neamtu-Halic *et al.*, 2019). However, it has not yet been used in a more fundamental HIT set up with a moderately large Reynolds number forcing exhibiting a broad range of vortex sizes.

Our aim here is to study the interaction of the worms with the surrounding flow based on an objective detection method that provides the boundaries of the structures and allows quantifying the exchange of mass, momentum and vorticity across them.

Description of the experimental data set

The experimental data set that is analyzed in this study is from the scanning particle image velocimetry (PIV) measurement of homogeneous turbulent flow between a pair of counter-rotating impellers in a large von Kármán mixing tank facility (Lawson & Dawson, 2014, 2015). A two-dimensional sketch of the facility with its dimensions and the theoretical flow pattern inside the tank is shown in figure 1. The facility is a dodecagonal tank made of Perspex with $2m$ height and $2m$ width. The diameter of the impellers is $1.6m$ and the vertical distance between the two impellers is about $1.25m$. The axisymmetric shear generated by the revolution of the impellers induces a secondary flow pattern because of the centrifugal pumping effect. The superposition of the primary flow pattern (axisymmetric shear) and the secondary flow pattern (centrifugal pumping) makes homogeneous turbulence at the center of the tank with almost zero mean velocity and high level of turbulent fluctuations. The Reynolds number of the flow based on the impeller radius $Re_{R_I} = \Omega_I R_I^2 / \nu$ is 23,000 where Ω_I is the rotational speed of the impellers, R_I is the radius of the impellers, and ν is the kinematic viscosity of the fluid. The Reynolds number based on Taylor micro-scale of the flow is $R_\lambda = 179$ and the Kolmogorov length scale is $\eta = 0.926mm$. The spatial resolution of the data set is about 1η . The non-dimensional volume of the flow is $L_x/\eta \times L_y/\eta \times L_z/\eta = 135 \times 134 \times 25.4$. In total, the data set consists of 1003 statistically independent volumes with long and random separation times between consecutive acquisitions. The detailed description of the volumetric scanning-PIV measurement technique that is used to achieve the velocity fields can be found in Lawson & Dawson (2014).

Objective Eulerian Coherent Structure definition and the detection method

To detect the fine-scale vortical structures objectively in the flow field the definition of Objective Eulerian Coherent Structure (OECS) proposed by Haller *et al.* (2016) has been

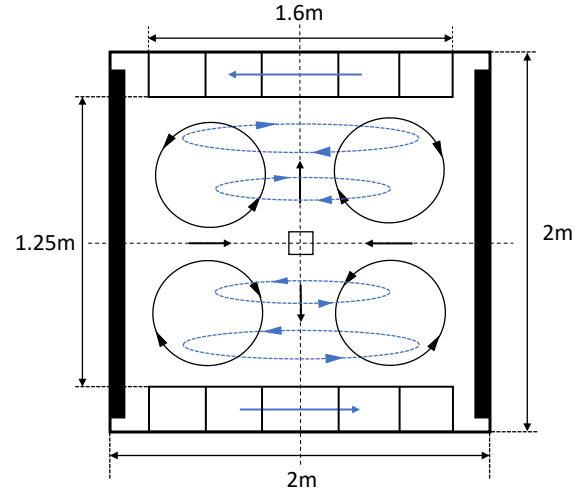


Figure 1. Schematic of the big von Kármán mixing flow facility.

implemented. The definition of OECS is based on Instantaneous Vorticity Deviation (IVD) scalar field.

$$IVD(x, t) = |\omega(x, t) - \bar{\omega}(t)| \quad (1)$$

where $\omega = \nabla \times u$ is the vorticity vector and $\bar{\omega}$ is the spatially averaged vorticity vector at each time step. OECS is defined as a nested family of level surfaces of IVD. The value of IVD does not increase when marching outwards from the center. The center has the maximum value of IVD and the boundary is defined as the outermost convex level surface. This definition of vortical structure is observer-independent and ensures instantaneous coherence of the rate of material bulk rotation relative to the mean background rotation (Haller *et al.*, 2016). An algorithm based on the presented definition has been developed and implemented to detect the three dimensional vortical structures. The algorithm is explained in details in Neamtu-Halic *et al.* (2019).

Burgers' vortex model

Since some features of the small-scale vortical structures are compared to the Burgers' vortex model, a short description of it is provided here. The Burgers' vortex model is an exact solution of incompressible Navier-Stokes equation by assuming that the vorticity field is unidirectional. It means that the vorticity field is either one dimensional or both the vorticity and strain fields are axisymmetric (Saffman, 1995). Burgers' vortices are stable as their radii do not change. Vorticity is produced by the inviscid phenomenon of vortex stretching ($\omega \cdot \nabla u$) inside the vortex and is diffused outward by the viscous phenomenon of vorticity diffusion ($\nu \nabla^2 \omega$). The competing effects of these phenomena lead to entrainment of fluid in radial direction into the vortex and detrainment of fluid along the axial direction to conserve rotational energy and mass (figure 2). Since an exact solution exists for the flow of Burgers' vortex, all the parameters related to the velocity field and velocity gradient tensor can be calculated analytically.

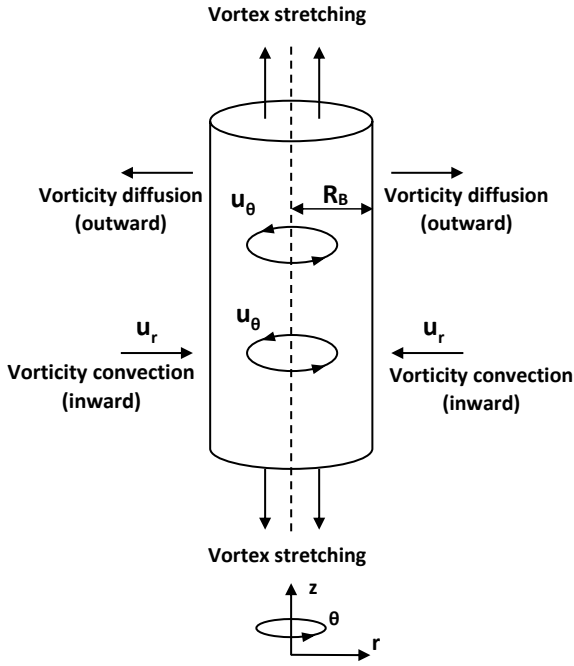


Figure 2. Burgers' vortex model.

RESULTS

In figure 3 the intense vortical structures in a snapshot of the experimental data set are shown. The black curved lines show the center of the structures and the pink surfaces show the boundary of each structure. In total, about 12500 structures have been detected over the 1003 snapshots of the data set. The average radius of the structures is 5.1η (figure 4) and were found to occupy 1.4% of the measurement volume which is in agreement with the DNS study of Jiménez *et al.* (1993).

The J-PDFs of enstrophy ($\omega^2 = \omega \cdot \omega$ where ω is the vorticity vector) and dissipation ($\varepsilon = 2\nu s_{ij}s_{ij}$ where $s_{ij} = \frac{1}{2}(\frac{\partial u_i}{\partial x_j} + \frac{\partial u_j}{\partial x_i})$ is the rate of strain tensor) are calculated for the whole volume of flow (figure 5) and within the structures (figure 6), separately. By comparing these J-PDFs one can see a shift towards the high-vorticity and low-strain quadrant for the points within the structures. Also, a noticeable preference can be seen for the J-PDF within the structures to get aligned with the diagonal line of the enstrophy-dissipation figure. This preference shows that the extreme events of enstrophy and dissipation scale together inside the structures.

Further insight can be gained by considering the alignment between the vorticity vector $\omega = (\omega_1, \omega_2, \omega_3)$ and the rate-of-strain eigenvectors $e = (e_1, e_2, e_3)$, where $\sigma_1 \geq \sigma_2 \geq \sigma_3$ are the corresponding eigenvalues, as it affects the vortex stretching phenomenon (production/destruction of enstrophy, $\omega_i \omega_j s_{ij}$) (Tsinober, 2009). For incompressible flows, from the continuity equation ($\frac{\partial u_i}{\partial x_i} = 0$) it can be concluded that $\sigma_1 + \sigma_2 + \sigma_3 = 0$. This means that $\sigma_1 > 0$ and $\sigma_3 < 0$ everywhere in a flow field and that the value of σ_2 can be either positive or negative depending on the value that the sum of σ_1 and σ_3 has ($\sigma_2 = -(\sigma_1 + \sigma_3)$). The alignments, $\cos(\theta_i) = e_i \cdot \frac{\omega}{|\omega|}$, are calculated for the whole volume of the flow and within the structures and shown in figure 7. For the case of the whole volume it can be seen

that the vorticity vector and the intermediate eigenvector are well-aligned with each other. The alignment between the vorticity vector and the compressive eigenvector was found and shows that these two vectors are mostly perpendicular to each other. However, the PDF of the alignment between the vorticity vector and the extensional eigenvector showed no preferential alignment. The preferential alignment between the vorticity and the intermediate strain eigenvector seems to be a universal feature of turbulent flows (Elsinga & Marusic, 2010). On the other hand, for the case of inside the structures it can be seen that the vorticity vector is also aligned with the intermediate eigenvector but it is normal to both extensional and compressive eigenvectors. So, one can interpret these structures as quasi 1-D with weak curvature because the vorticity vectors inside them have a strong preference to be aligned with the intermediate eigenvector and to be normal to the rest of the eigenvectors (Tsinober, 2009). As it was discussed earlier, the intermediate eigenvalue σ_2 can take either positive or negative values. For the case of the structures, since the vorticity vector has a strong preference to be only aligned with the intermediate eigenvalue the sign that σ_2 takes determines if the dominant topological phenomenon is vortex stretching ($\omega_i \omega_j s_{ij} > 0$) or vortex compression ($\omega_i \omega_j s_{ij} < 0$). Figure 8 shows PDFs of the three eigenvalues of the rate of strain tensor for both the cases of whole volume and inside the structures. The PDFs of the eigenvalues for the case of inside the structures have wider tails compared to the whole volume of flow. This means that these structures are intense realization of vortex stretching/compression in the flow field. As it is expected the value of σ_1 is only positive and the value of σ_3 is only negative. For σ_2 it can be seen that both negative and positive values are probable but on average it is positive for the both cases of whole volume and inside the structures ($\langle \frac{\sigma_2}{(\omega^2)^{0.5}} \rangle > 0$). It can be concluded that these structures are stretched on average by the strain field of the flow.

Since these intense vortex filaments tend to be embedded in a more quiescent (i.e. mostly characterized by rather weak enstrophy) flow, we can treat the boundary of the vortex filaments as an internal interface (Eisma *et al.*, 2015; Ishihara *et al.*, 2013), analogous to the turbulent/non-turbulent interface of free shear flows and evaluate whether they entrain and/or detrains flow. To investigate this, a formula for calculating the entrainment velocity, v_n , derived by Holzner & Lüthi (2011) is used (equation 2):

$$v_n = -\frac{2\omega_i \omega_j s_{ij}}{|\nabla \omega^2|} - \frac{\nu \frac{\partial^2 \omega^2}{\partial x_j \partial x_j}}{|\nabla \omega^2|} + \frac{2\nu \frac{\partial \omega_i}{\partial x_j} \frac{\partial \omega_j}{\partial x_i}}{|\nabla \omega^2|} \quad (2)$$

Here the entrainment velocity, v_n , is defined as $v_n n = u^s - u$ where u^s is the velocity of an isosurface element, u is the flow velocity at that isosurface, and $n = \frac{\nabla \omega^2}{|\nabla \omega^2|}$ is the normal vector to the isosurface. According to this definition, when $v_n \leq 0$ fluid elements at the isosurface are entrained into the structure and when $v_n > 0$ fluid elements are detrained out of the structure (Mistry *et al.*, 2019). Figure 9 shows the entrainment velocity and its components in equation 2 evaluated on the boundary of the structures. The entrainment velocity is negative on average which means that the structures are entraining ambient fluid on average. To conserve mass the same amount of fluid needs to be detrained axially in order to preserve the total volume of the vortices. Furthermore, by comparing the different terms in the entrainment velocity

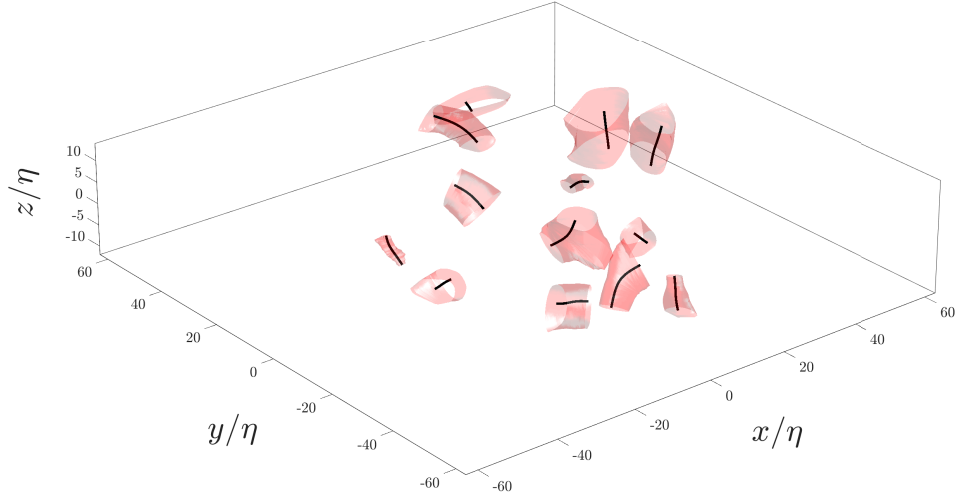


Figure 3. Example of OECSs in a snapshot of the experimental data set. Dimensions are normalized by the Kolmogorov length scale.

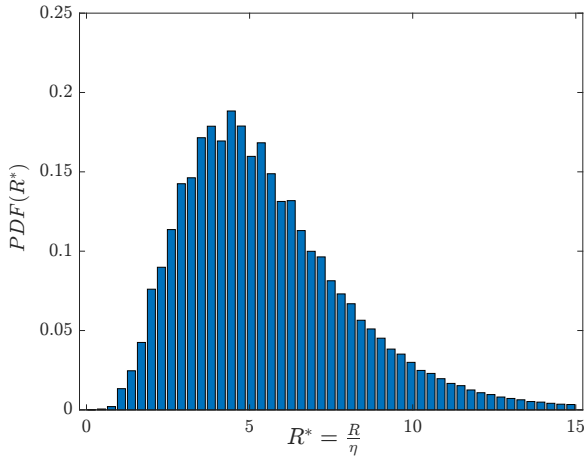


Figure 4. PDF of normalized radius of the structures.

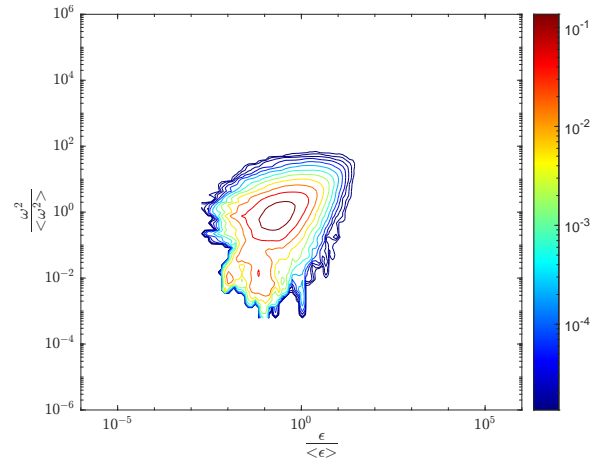


Figure 6. J-PDF of normalized enstrophy and dissipation for the structures.

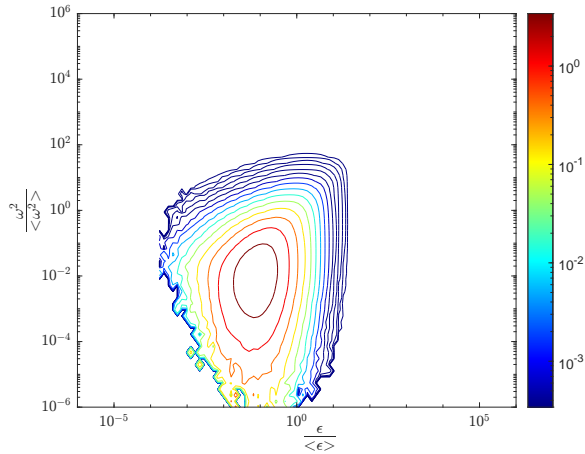


Figure 5. J-PDF of normalized enstrophy and dissipation for the whole volume.

equation we can see that the average entrainment results from a competition between inviscid and viscous effects. Figure 9 shows that local entrainment ($\frac{v_n}{u_\eta} \leq 0$) happens where local vortex stretching is greater than vorticity diffusion. On the other hand, detrainment ($\frac{v_n}{u_\eta} > 0$) occurs when the summation of local effects of vorticity diffusion and dissipation are

greater than the local vortex stretching. This behaviour is consistent with a stable Burgers' vortex model where the ambient fluid is entrained to the vortex from the boundary in radial direction, $u_r = -\frac{\alpha}{2}r < 0$, and that the vortex remains stable because of the balance between inviscid and viscous phenomena acting on it.

To further investigate the importance of different physical phenomena in the vortical structures and to compare them with the Burgers' vortex model, all the terms in enstrophy transport equation (equation 3) are calculated along the radial lines of the structures. This equation implies that the rate of change of enstrophy (the material derivative, $\frac{D\omega^2}{Dt} = \frac{\partial \omega^2}{\partial t} + u_j \frac{\partial \omega^2}{\partial x_j}$) describes a competition between inviscid vortex stretching ($2\omega_i \omega_j s_{ij}$), the viscous diffusion of enstrophy ($\nu \frac{\partial^2 \omega^2}{\partial x_j \partial x_j}$), and enstrophy dissipation ($-2\nu \frac{\partial \omega_i}{\partial x_j} \frac{\partial \omega_j}{\partial x_i}$). Figure 10 plots the averaged values of these terms conditioned on radial directions of the structures. The terms are normalized by t_η^3 where $t_\eta = (\frac{\nu}{\epsilon})^{1/2}$ is the Kolmogorov time scale. The horizontal axis of the plot represents the normalized radius of the structures. For each radial line, the radial distance from the center (r) is normalized by the local radius of the structure (R).

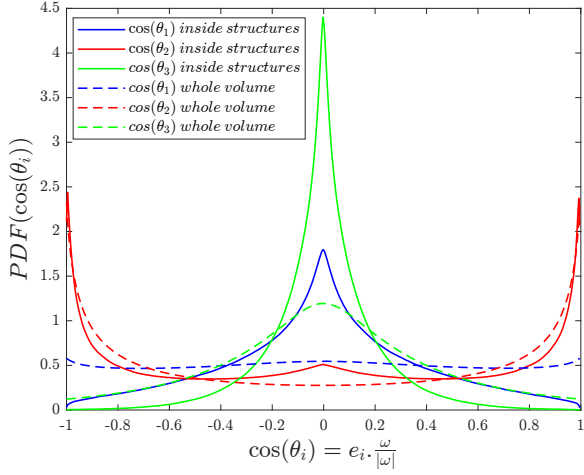


Figure 7. Alignment between the vorticity vector and the eigenvectors of the rate of strain tensor.

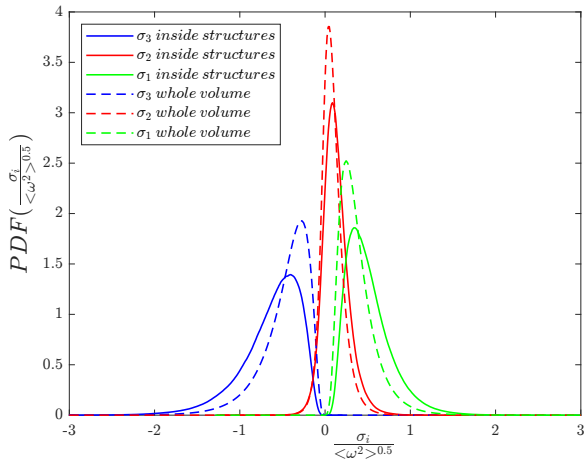


Figure 8. PDFs of eigenvalues of the rate of strain tensor for the whole volume of the flow and inside the vortical structures.

$$\frac{D\omega^2}{Dt} = 2\omega_i\omega_j s_{ij} + \nu \frac{\partial^2 \omega^2}{\partial x_j \partial x_j} - 2\nu \frac{\partial \omega_i}{\partial x_j} \frac{\partial \omega_i}{\partial x_j} \quad (3)$$

Figure 10 shows that near the center of the structures ($\frac{r}{R} = 0$), enstrophy diffusion is more dominant than both vortex stretching and enstrophy dissipation, the latter of which has relatively small values resulting in $\frac{D\omega^2}{Dt} < 0$. By marching towards the boundary from the center both vortex stretching and enstrophy diffusion become weaker as dissipation gradually increases. The rate of change of diffusion is faster than vortex stretching which results in $\frac{D\omega^2}{Dt} > 0$ after $\frac{r}{R} \approx 0.2$. Dissipation reaches a maximum near the boundary of the structures. As $\frac{r}{R} > 1$, all the terms become constant (flat). To compare the behaviour with Burgers' vortex model, equivalent Burgers' vortices are considered and the same terms of the equation are calculated and plotted in figure 11. The equivalent Burgers' vortices are achieved by calculating stretching (α_0) and enstrophy (ω_0^2) at the center of the structures. By knowing α_0 and ω_0^2 and using the analytical relations available for Burgers' vortex model all the desired terms can be calculated. By comparing figures 10 and 11 a similar competition between the different terms in the enstrophy transport equation can be

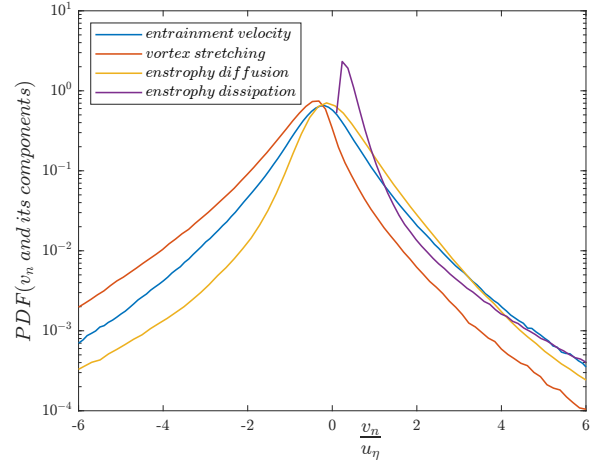


Figure 9. PDFs of entrainment velocity, v_n , at the boundary of the structures and its components.

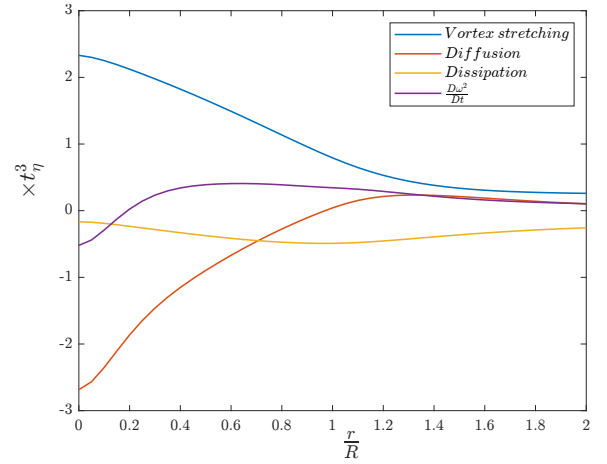


Figure 10. Averaged enstrophy transport equation terms conditioned on radial lines inside the structures.

observed although with some small changes in their magnitude which shows that, on average the Burgers' vortex model reproduces the dominant physics of the small-scale structures quite well.

SUMMARY & CONCLUSIONS

In this study, features of small-scale vortical structures ('worms') in a fully resolved 3D-3C experimental data set of homogeneous axisymmetric turbulence with $Re_\lambda = 179$ measured at the center of a large-scale von Kármán mixing tank are investigated. To avoid the arbitrariness in the definition of vortices (thresholding), an objective definition based on Objective Eulerian Coherent Structure (OECS) proposed by Haller *et al.* (2016) is implemented to detect the vortices in the volumetric velocity fields. In total, 12500 vortices were detected in 1003 volumes of the turbulent flow. The average radius of the structures is $\langle R \rangle = 5.1\eta$ that is in agreement with $\langle R \rangle \approx 5\eta$ widely reported in the literature for DNS studies. Small-scale vortex structures were found to occupy 1.4% of the volume of the flow in agreement with $\sim 1\%$ reported in the literature from DNS. Joint PDFs of enstrophy and dissipation within the volume and conditioned inside the structures were showed that the values of enstrophy and dissipation are concentrated in the small-scale vortices compared to the whole

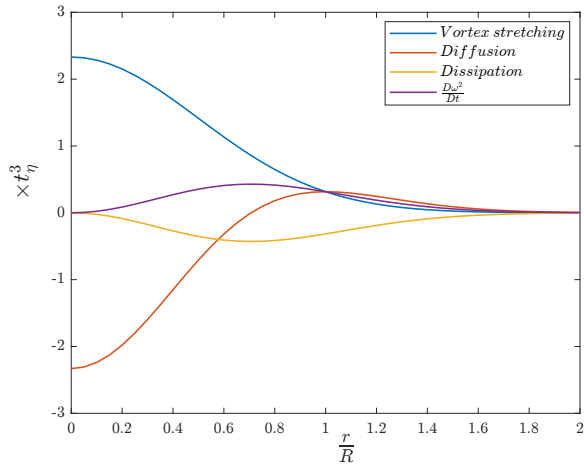


Figure 11. Averaged enstrophy transport equation terms of the equivalent Burgers' vortex model conditioned on radial lines inside the structures.

flow field and that they scale inside the structures. The alignment of the vorticity vector and eigenvectors of the rate of strain tensor showed the vorticity vector has a strong tendency to be aligned with the intermediate eigenvector and be normal to the compressive and extensional eigenvectors as found in previous turbulent flows. Since the average value of the intermediate eigenvalue is positive ($\langle \sigma_2 \rangle > 0$) vortex stretching is the dominant topological phenomenon.

To investigate the exchange of mass by the small-scale vortices, the entrainment velocity equation was solved on the boundary of the structures showing that they, on average, entrain relatively ambient flow from the surroundings. The total volume of the structures does not change in homogeneous stationary turbulence, the mass entrainment is compensated by the mass outflow along the axial direction. It is also shown that the local entrainment/detrainment at the boundary is the result of a competition between inviscid and viscous phenomena. This exchange of mass is accompanied with exchange of momentum, energy, and enstrophy with the ambient fluid. Therefore the structures are not passive in this sense. Finally, the enstrophy transport equation conditioned on radial lines of the vortices was studied and compared to those of equivalent Burgers' vortices. The results indicate that Burgers' vortex model on average reasonably captures the flow physics of the vortex structures.

REFERENCES

Dubief, Yves & Delcayre, Franck 2000 On coherent-vortex identification in turbulence. *Journal of Turbulence* **1**.
Eisma, Jerke, Westerweel, Jerry, Ooms, Gijs & Elsinga, Ger-

rit E. 2015 Interfaces and internal layers in a turbulent boundary layer. *Physics of Fluids* **27** (5).
Elsinga, G. E. & Marusic, I. 2010 Universal aspects of small-scale motions in turbulence. *Journal of Fluid Mechanics* **662**, 514–539.
Ganapathisubramani, B., Lakshminarasimhan, K. & Clemens, N. T. 2008 Investigation of three-dimensional structure of fine scales in a turbulent jet by using cinematographic stereoscopic particle image velocimetry. *Journal of Fluid Mechanics* **598**, 141–175.
Haller, G., Hadjighasem, A., Farazmand, M. & Huhn, F. 2016 Defining coherent vortices objectively from the vorticity. *Journal of Fluid Mechanics* **795**, 136–173.
Holzner, M. & Lüthi, B. 2011 Laminar superlayer at the turbulence boundary. *Phys Rev Lett* **106** (13), 134503.
Ishihara, Takashi, Kaneda, Yukio & Hunt, Julian C. R. 2013 Thin shear layers in high reynolds number turbulence—dns results. *Flow, Turbulence and Combustion* **91** (4), 895–929.
Jiménez, Javier & Wray, Alan A. 1998 On the characteristics of vortex filaments in isotropic turbulence. *Journal of Fluid Mechanics* **373**, 255–285.
Jiménez, Javier, Wray, Alan A., Saffman, Philip G. & Rogallo, Robert S. 1993 The structure of intense vorticity in isotropic turbulence. *Journal of Fluid Mechanics* **255**, 65–90.
Kang, Shin-Jeong, Tanahashi, Mamoru & Miyauchi, Toshio 2009 Dynamics of fine scale eddy clusters in turbulent channel flows. *Journal of Turbulence* **8**.
Lawson, John M. & Dawson, James R. 2014 A scanning piv method for fine-scale turbulence measurements. *Experiments in Fluids* **55** (12).
Lawson, J. M. & Dawson, J. R. 2015 On velocity gradient dynamics and turbulent structure. *Journal of Fluid Mechanics* **780**, 60–98.
Mistry, Dhiren, Philip, Jimmy & Dawson, James R. 2019 Kinematics of local entrainment and detrainment in a turbulent jet. *Journal of Fluid Mechanics* **871**, 896–924.
Neamtu-Halic, Marius M., Krug, Dominik, Haller, George & Holzner, Markus 2019 Lagrangian coherent structures and entrainment near the turbulent/non-turbulent interface of a gravity current. *Journal of Fluid Mechanics* **877**, 824–843.
Neamtu-Halic, M. M., Mollicone, J. P., van Reeuwijk, M. & Holzner, M. 2021 Role of vortical structures for enstrophy and scalar transport in flows with and without stable stratification. *Journal of Turbulence* pp. 1–20.
Saffman, Philip G 1995 *Vortex dynamics*. Cambridge university press.
da Silva, Carlos B., dos Reis, Ricardo J. N. & Pereira, José C. F. 2011 The intense vorticity structures near the turbulent/non-turbulent interface in a jet. *Journal of Fluid Mechanics* **685**, 165–190.
Tsinobor, Arkady 2009 *An informal conceptual introduction to turbulence*, , vol. 483. Springer.